Shadowing effects on the nuclear suppression factor, R_{dAu}, in $d+$Au interactions

R. Vogt

Nuclear Science Division, Lawrence Berkeley National Laboratory, Berkeley, California 94720, USA
and Physics Department, University of California, Davis, California 95616, USA

We explore how nuclear modifications to the nucleon parton distributions affect production of high-transverse-momentum hadrons in deuteron-nucleus collisions. We calculate the charged hadron spectra to leading order using standard fragmentation functions and shadowing parametrizations. We obtain the $d+$Au to pp ratio both in minimum bias collisions and as a function of centrality. The minimum bias results agree reasonably well with the BRAHMS data while the calculated centrality dependence underestimates the data and is a stronger function of p_T than the data indicate.

One of the most intriguing results from the Relativistic Heavy Ion Collider (RHIC) at Brookhaven National Laboratory has been the suppression of hadrons with high transverse momentum p_T in central Au+Au collisions at center-of-mass energies $\sqrt{S_{NN}}$ of 130 and 200 GeV. The AA suppression factor

$$R_{AA}(p_T) = \frac{d\sigma_{AA}/dp_T}{\langle \sigma_{NN}^{\text{in}} T_{AA} \rangle d\sigma_{pp}/dp_T} \tag{1}$$

compares the AA and pp p_T distributions of hadrons, normalized by the number of binary collisions $\langle \sigma_{NN}^{\text{in}} T_{AA} \rangle$, the product of the nucleon-nucleon inelastic cross section σ_{NN}, and the nuclear overlap function T_{AA}. Saturation effects in the initial nuclear wave function and final-state parton energy loss were both proposed as explanations of the large suppression seen in Au+Au collisions by PHENIX [1,2], STAR [3,4], and BRAHMS [5]. To determine whether the suppression is an initial- or final-state effect, $d+$Au collisions at $\sqrt{S_{NN}} = 200$ GeV were recently studied at RHIC. The data [6–8] show that, at midrapidity ($\eta \approx 0$), the $d+$Au suppression factor

$$R_{dAu}(p_T) = \frac{d\sigma_{dAu}/dp_T}{\langle \sigma_{NN}^{\text{in}} T_{dAu} \rangle d\sigma_{pp}/dp_T} \tag{2}$$

is much closer to unity. These results suggest that the strong suppression in Au+Au collisions is a final-state effect, implying that, at least at central rapidities, saturation effects are small. However, at higher rapidities where the nuclear parton momentum fraction x_2 is smaller, such effects might still be important. Since x is not very small at RHIC, it is necessary to check if other, more conventional, models of nuclear shadowing may also explain the data.

The BRAHMS Collaboration has measured R_{dAu} at several values of pseudorapidity η and observed increasing suppression as η increases from $|\eta| \leq 0.2$ to $\eta = 3.2$ [8]. The BRAHMS measurements are in four η bins: $|\eta| \leq 0.2$, $0.8 \leq \eta \leq 1.2$ ($\eta = 1$), $1.9 \leq \eta \leq 2.35$ ($\eta = 2.2$), and $2.9 \leq \eta \leq 3.5$ ($\eta = 3.2$), corresponding to center-of-mass scattering angles $\theta_{\text{c.m.}}$ of $101.4° \geq \theta_{\text{c.m.}} \geq 78.6°$, $48.4° \geq \theta_{\text{c.m.}} \geq 33.5°$, $17.01° \geq \theta_{\text{c.m.}} \geq 10.9°$, and $6.3° \geq \theta_{\text{c.m.}} \geq 3.5°$, respectively. These data have also been divided into three centrality bins: (0–

20)%, (30–50)%, and (60–80)% of the geometric cross section. Using a Glauber calculation of the nuclear overlap with a Woods-Saxon density distribution for the gold nucleus and the Hulthén wave function to calculate the deuteron density, we find that these bins correspond to the impact parameter b ranges of $0 \leq b \leq 3.81$ fm, $4.66 \leq b \leq 6.01$ fm, and $6.59 \leq b \leq 7.74$ fm, respectively. Our calculated values of $\langle \sigma_{NN}^{\text{in}} T_{dAu} \rangle$ in these impact parameter bins are in relatively good agreement with those determined by BRAHMS. The results in the two lowest η bins are reported for $(h^+ + h^-)/2$ while the $\eta = 2.2$ and 3.2 bins are reported for h^- only, where h^+ and h^- stand for the positively and negatively charged hadrons, respectively.

In this paper, we calculate $R_{dAu}(p_T)$ in the BRAHMS η bins using two parametrizations of nuclear shadowing. We also calculate the central-to-peripheral ratios $R_{\text{CP}}(p_T)$ with two parametrizations of the spatial dependence of shadowing. The calculated ratios are compared to the BRAHMS data [8]. To better illustrate the effects of shadowing alone, we do not include the Cronin effect, p_T broadening [9,10], in our calculations.

We make a leading order (LO) calculation of minijet production to obtain the yield of high-p_T partons [11]. The p_T distribution of Ref. [12] is modified to include the nuclear parton distribution functions,

$$\frac{d\sigma_{dAu \to hX}}{d^2b\, dp_T} = 2p_T \sum_{i,j=q,\bar{q},g} \int_{\theta_{\min}}^{\theta_{\max}} \frac{d\theta_{\text{c.m.}}}{\sin \theta_{\text{c.m.}}} \int dx_1 \int dx_2 \int d^2s$$

$$\times \int dz \int dz'\, F_{i/d}(x_1, Q^2, \vec{s}, z)$$

$$\times F_{j/\text{Au}}(x_2, Q^2, |\vec{b} - \vec{s}|, z') \frac{D_{h/k}(z_c, Q^2)}{z_c} \frac{d\hat{\sigma}_{ij \to k}}{d\hat{t}}, \tag{3}$$

where x_1 and x_2 are the parton momentum fractions in the deuterium and gold nuclei, respectively, Q is the momentum scale of the hard interaction, and z_c is the fraction of the parton momentum transferred to the final-state hadron. The integrals over center-of-mass scattering angle $\theta_{\min} \leq \theta_{\text{c.m.}} \leq \theta_{\max}$ correspond to the BRAHMS angular regions, given

previously. The $2 \rightarrow 2$ minijet cross sections $d\hat{\sigma}_{ij \rightarrow k}/d\hat{t}$ are given in Ref. [13]. Even though the next-to-leading order corrections may affect the shape of the p_T distributions, the higher-order corrections should largely cancel out in R_{dAu}, as is the case for J/ψ [14] and Drell-Yan [11] production.

The parton densities in the gold nucleus, $F_{j/Au}(x, Q^2, \vec{b}, z)$, can be factorized into x- and Q^2-independent nuclear density distributions, position- and nuclear-number-independent nucleon parton densities, and a shadowing function $S_{P,S}^j(A, x, Q^2, \vec{b}, z)$ that describes the modification of the nuclear parton distributions in position and momentum space. The first subscript on the shadowing function, P, refers to the shadowing parametrization while the second, S, to the spatial dependence. Most available shadowing parametrizations ignore effects in deuterium so that $F_{i/d}$ depends only on the deuterium density distribution and the nucleon parton densities. We account for the proton and neutron numbers of both nuclei. Then [14]

$$F_{i/d}(x, Q^2, \vec{s}, z) = \rho_d(\vec{s}, z) f_{i/N}(x, Q^2), \quad (4)$$

$$F_{j/Au}(x, Q^2, |\vec{b} - \vec{s}|, z') = \rho_{Au}(|\vec{b} - \vec{s}|, z') \\ \times S_{P,S}^j(Au, x, Q^2, |\vec{b} - \vec{s}|, z') f_{j/N}(x, Q^2), \quad (5)$$

where $f_{i/N}(x, Q^2)$ is the nucleon parton density. In the absence of nuclear modifications, $S_{P,S}^j \equiv 1$. The nucleon density distribution of the gold nucleus is assumed to be a Woods-Saxon with $R_{Au} = 6.38$ fm [15]. We use the Hulthén wave function [16] to calculate the deuteron density distribution. The densities are normalized so that $\int d^2s \, dz \, \rho_A(\vec{s}, z) = A$. We use the Martin-Roberts-Stirling-Thorne (MRST) LO parton distributions [17] for isolated nucleons and take $Q^2 = p_T^2$.

We have chosen two parametrizations of nuclear shadowing which cover extremes of gluon shadowing at low x. The Eskola *et al.* parametrization EKS98 is based on the Gluck-Reya-Vogt (GRV) LO [18] parton densities. At the minimum scale Q_0^2, valence quark shadowing is identical for u and d quarks. Likewise, $\bar{u}$, $\bar{d}$, and $\bar{s}$ shadowing is identical at Q_0^2. Even though the light quark shadowing ratios are not constrained to be equal at higher scales, the differences between them are small. Shadowing of the heavier flavor sea, $\bar{s}$ and higher, is calculated separately at Q_0^2. The shadowing ratios for each parton type are evolved to LO for $2.25 < Q^2 < 10^4$ GeV and are valid for $x \geq 10^{-6}$ [19,20]. Interpolation in nuclear mass number allows results to be obtained for any input A. The parametrizations by Frankfurt, Guzey, and Strikman combine Gribov theory with hard diffraction [21]. They are based on the CTEQ5M [22] parton densities and evolve each parton species separately to next-to-leading order (NLO) for $4 < Q^2 < 10^4$ GeV. Although the x range is $10^{-5} < x < 0.95$, the sea quark and gluon ratios are unity for $x > 0.2$. The EKS98 valence quark shadowing ratios are used as input since Gribov theory does not predict valence shadowing. The parametrizations are available for four different values of A: 16, 40, 110, and 206. We use $A = 206$ for the

gold nucleus with the parametrization that gives the strongest gluon shadowing for the largest contrast to EKS98, denoted FGS1 here.

We now turn to the spatial dependence of the shadowing. Since some qualitative spatial dependence has been observed [23] but the exact behavior is unknown, we have tried two different parametrizations for inhomogeneous shadowing in $d + Au$ collisions [11,24–26]. The first, $S_{P,WS}^j$, assumes that shadowing is proportional to the local density $\rho_A(r)$,

$$S_{P,WS}^j(A, x, Q^2, \vec{s}, z) = 1 + N_{WS}[S_P^j(A, x, Q^2) - 1]\frac{\rho_A(r)}{\rho_A(0)}, \quad (6)$$

where $r = \sqrt{s^2 + z^2}$, $\rho_A(0)$ is the central density, and N_{WS} is chosen so that $(1/A) \int d^2s \, dz \, \rho_A(\vec{s}, z) S_{P,WS}^j = S_P^j$. When $r \gg R_A$, the nucleons behave as free particles while, at the center of the nucleus, the modifications are larger than S_P^i.

If, instead, shadowing stems from multiple interactions of the incident parton [27], parton-parton interactions are spread longitudinally over the coherence length $l_c = 1/2m_N x$, where m_N is the nucleon mass [28]. For $x < 0.016$, $l_c > R_A$ for any A and the incident parton interacts coherently with all the target partons in its path so that

$$S_{P,\rho}^j(A, x, Q^2, \vec{s}, z) = 1 + N_\rho[S_P^j(A, x, Q^2) - 1]\frac{\int dz \, \rho_A(\vec{s}, z)}{\int dz \, \rho_A(0, z)}. \quad (7)$$

The integral over z includes the material traversed by the incident nucleon. The normalization requires $(1/A) \int d^2s \, dz \, \rho_A(\vec{s}, z) S_{P,\rho}^j = S_P^j$ with $N_\rho > N_{WS}$. At large x, $l_c \ll R_A$ and shadowing is proportional to the local density, Eq. (6).

While there are three homogeneous FGS parametrizations, only two inhomogeneous parametrizations are provided. No spatial dependence is given for FGS1, the case with the strongest gluon shadowing. We have checked the available dependencies against those calculated using $S_{FGS1,WS}^j$ and $S_{FGS1,\rho}^j$ and found that, at similar values of the homogeneous shadowing ratios, $S_{FGS1,\rho}^j$ is quite compatible with the available FGS inhomogeneous parametrizations. Therefore, to characterize the spatial dependence of FGS1, we use $S_{FGS1,\rho}^j$.

The fragmentation functions $D_{h/k}(z_c, Q^2)$ describe the production of hadron h from parton k with $z_c = p_h/p_k$. The produced partons are fragmented into charged pions, kaons, and protons using the LO Kniehl-Kramer-Pötter (KKP) fragmentation functions [29], fitted to e^+e^- data. The final-state hadrons are assumed to be produced pairwise so that $\pi \equiv (\pi^+ + \pi^-)/2$, $K \equiv (K^+ + K^-)/2$, and $p \equiv (p + \bar{p})/2$. The equality of p and $\bar{p}$ production obviously does not describe low-energy hadroproduction well. At higher energies, however, the approximation that $p = \bar{p}$ may be more reasonable. The produced hadrons follow the parent parton direction. The minimum Q^2 in the KKP fragmentation functions is $Q_{Fr_0}^2 = 2$ GeV^2, similar to but somewhat lower than the minimum Q^2 of the shadowing parametrizations. Thus the minimum p_T of our calculations is $\sqrt{2}$ GeV. We assume the same scale in the parton densities and the fragmentation functions, Q^2

$=Q_{\mathrm{Fr}}^2 = p_T^2$. A larger scale, p_T^2/z_c^2, is sometimes used in the parton densities but where z_c is large, as is the case here, changing the scale does not significantly alter the calculated ratios.

The largest contribution to the total final-state charged particle production is from the charged pions, followed by the kaons. The proton contribution is the smallest even though, in $d+$Au collisions at RHIC, $(p+\bar{p})/h \approx 0.24 \pm 0.02$ where $h = h^+ + h^-$ for $2 < p_T < 3$ GeV, independent of centrality [30]. The $d+$Au result is similar to that from pp, 0.21 ± 0.01 [30]. The discrepancy between the RHIC $d+$Au and pp results and the extrapolation from e^+e^- is due to the poor knowledge of the fragmentation functions at large z_c.

We have calculated the p_T distributions for final-state charged pions, kaons, and protons/antiprotons separately as well as the sum of all charged particles. For each final-state hadron, we determine the fraction of the total from produced quarks, antiquarks, and gluons. In the central η bin for pion production, gluons are produced almost equally in the $gg \rightarrow gg$ and $qg \rightarrow qg$ channels. The qg channel is somewhat larger for $p_T > 5$ GeV. There is a negligible contribution from $q\bar{q} \rightarrow gg$. Pion production by quarks and antiquarks proceeds mainly through the $qg \rightarrow qg$ channel for quarks and $\bar{q}g \rightarrow \bar{q}g$ for antiquarks. The next largest contributions to pion production by quarks are the $qq' \rightarrow qq'$ and $qq \rightarrow qq$ channels which are of very similar strength, followed by $q\bar{q} \rightarrow q\bar{q}$ and $gg \rightarrow q\bar{q}$ with a negligible contribution from $q\bar{q} \rightarrow q'\bar{q}'$. The contributions to antiquark production after $\bar{q}g \rightarrow \bar{q}g$ are $\bar{q}q' \rightarrow \bar{q}q'$, $\bar{q}q \rightarrow \bar{q}q$, and $gg \rightarrow q\bar{q}$, followed by smaller contributions from $\overline{qq} \rightarrow \overline{qq}$ and $q\bar{q} \rightarrow q'\bar{q}'$. Similar results are found for kaon and proton production. However, the proton distributions fall off more steeply with p_T.

The relative contributions from the production channels remain similar as rapidity increases. The most important change is in gluon production where the $qg \rightarrow qg$ channel grows more dominant, finally becoming larger than the $gg \rightarrow gg$ channel for all p_T for $\eta=3.2$. Indeed, at the most forward rapidity, the $q\bar{q} \rightarrow gg$ channel becomes comparable to the qg channel at $p_T \sim 8$ GeV. This may seem counterintuitive since the ion x_2 value decreases as η grows, increasing the gluon density. However, the deuteron x_1 value increases more rapidly and, at large η, we are in a region where the deuteron gluon density is dropping steeply while the quark density, particularly that of the valence quarks, is still significant. Thus the qg channel is more important than the gg channel at large η, particularly when p_T and x_1 are large. Also, at high η and p_T, $p_T > 7.5$ GeV, antiquarks are predominantly produced by valence quark induced processes since these are large at high x.

Because we begin to approach the edge of phase space with increasing η, the p_T distributions steepen, especially for antiquark and gluon production. Quark production, which includes the valence contribution, dominant at high p_T and η, remains harder overall. Thus quark production will come to dominate all final-state hadron production. This effect, increasingly important at high p_T and η, is reflected in the relative contributions to pion, kaon, and proton production by quarks, antiquarks, and gluons. At $|\eta| \leq 0.2$, pion production is dominated by produced gluons up to $p_T > 9$ GeV where pion production by quarks becomes larger. Gluon pro-

TABLE I. The average values of the Au and d momentum fractions, $\langle x_2 \rangle$ and $\langle x_1 \rangle$, respectively, as well as the average fraction of the final-state parton momentum transferred to the hadron, $\langle z_c \rangle$, in the four BRAHMS pseudorapidity intervals. The minimum values correspond to $p_T \approx \sqrt{2}$ GeV while the maximum corresponds to $p_T = 12$ GeV for the first three η bins and 10 GeV for the most forward η bin.

$\langle \eta \rangle$	$\langle x_2 \rangle$		$\langle x_1 \rangle$		$\langle z_c \rangle$	
	min	max	min	max	min	max
≈ 0	0.07	0.22	0.07	0.22	0.52	0.64
1	0.055	0.18	0.1	0.33	0.54	0.68
2.2	0.042	0.14	0.17	0.62	0.55	0.81
3.2	0.035	0.23	0.32	0.95	0.64	0.96

duction of kaons is rather small, similar to the quark contribution at $p_T \sim Q_{\mathrm{Fr}_0}$ but dropping below the antiquark contribution at $p_T \sim 3.5$ GeV. Quark production is most important for protons at $p_T > 3.5$ GeV. As η increases, quark production of final-state hadrons becomes increasingly dominant. Already at $\eta=1$, more than half of all kaons and protons are produced by quarks for $p_T > 2.5$ GeV. At higher η, antiquarks and gluons make negligible contributions to low-p_T kaon and proton production at $\eta=2.2$ and 3.2. Quarks also dominate pion production for $p_T > 6.5$, 3, and 1.5 GeV with $\eta=1$, 2.2, and 3.2, respectively.

We have calculated the average Au ion momentum fraction $\langle x_2 \rangle$ and the average deuteron momentum fraction $\langle x_1 \rangle$ for $\sqrt{2} \leq p_T \leq 12$ GeV. However, the largest accessible p_T decreases to 9.5 GeV at $\eta=3.2$ due to phase space. The results are shown in Table I. Since these are average x_2 values, the actual x_2 for each event can be smaller or larger than these averages. The minimum and maximum $\langle x_2 \rangle$ correspond to the lowest and highest p_T values, respectively. Both the minimum and maximum values decrease as η increases so that the minimum $\langle x_2 \rangle$ is reached at $\eta=3.2$. However, the maximum $\langle x_2 \rangle$ increases relative to more central η values due to the reduction of phase space at high p_T. Note that as $\theta \rightarrow 0$, $\langle x_2 \rangle \rightarrow 1$. The averages are not very sensitive to changes in the parton densities or the choice of factorization, renormalization, or fragmentation scales.

The total hadron yield closely follows that of the pions. There is little variation of $\langle x_2 \rangle$ between hadron species although the proton averages are generally somewhat smaller than those of the mesons. A small difference between the partonic contributions to hadron production can be attributed to the behavior of the parton distribution functions in the various production channels. A set of LO parton densities derived including the GLRMQ recombination terms at low x found deviations from normal Dokshitzer-Gribov-Lipatov-Altavelli-Parcsi (DGLAP) evolution at $x < 10^{-3}$ for the proton [31]. Thus one may question whether saturation effects can be at work here when $\langle x_2 \rangle = 0.035$ at $\eta=3.2$.

While the average Au momentum fraction is decreasing with centrality, the average deuteron momentum fraction x_1 is increasing. Note that the maximum $\langle x_1 \rangle$ at $\eta=3.2$ approaches 1, indicative of the edge of phase space. The aver-
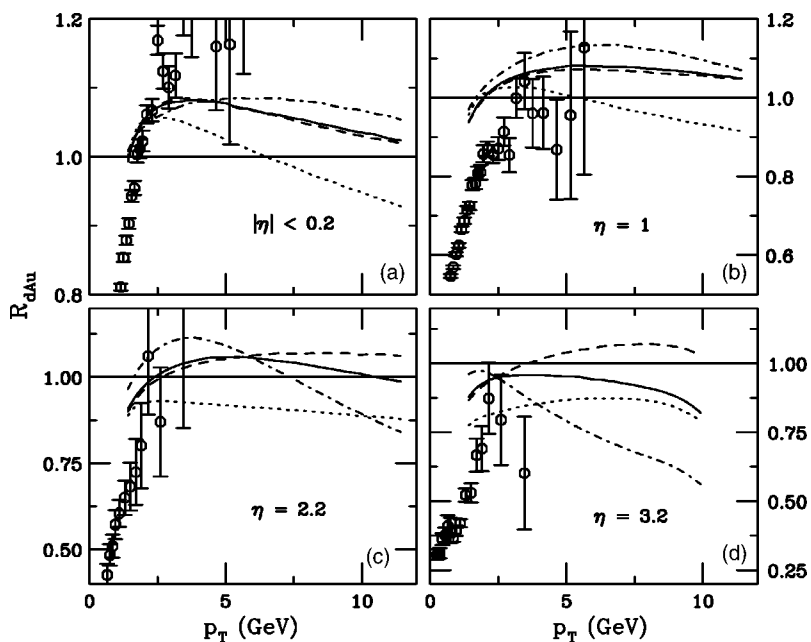
FIG. 1. $R_{d\mathrm{Au}}$ for charged pions (dashed) and kaons (dot-dashed) as well as protons and antiprotons (dotted), and the sum over all charged hadrons (solid) for deuteron-gold collisions at $\sqrt{S_{NN}}=200$ GeV as a function of p_T. The results for homogeneous shadowing with the EKS98 parametrization are compared to the minimum bias BRAHMS data [8] in the following η bins: (a) $|\eta| \leq 0.2$; (b) $\eta=1$; (c) $\eta=2.2$; and (d) $\eta=3.2$.

age z_c in the fragmentation functions is large, ≈ 0.5 at midrapidity, and increasing with η and p_T. The fragmentation functions are best determined for smaller z_c so that the high-z_c fragmentation functions are unreliable, especially for baryon production. Modeling of high-p_T and high-η hadron production thus contains large theoretical uncertainties due to the fragmentation functions. There is more variation in $\langle z_c \rangle$ due to parton type than in $\langle x_2 \rangle$. The proton $\langle z_c \rangle$ tends to be somewhat smaller than for pions or kaons. The tabulated values are for total charged hadrons.

We now compare the ratios $R_{d\mathrm{Au}}$ calculated for the two homogeneous shadowing parametrizations, to the BRAHMS data [8]. The EKS98 results are shown for each η interval in Fig. 1 while those employing the FGS1 parameterization are

shown in Fig. 2. We show the results for charged pions (dashed), charged kaons (dot-dashed), and protons/antiprotons (dotted) separately. The solid curves give the total charged hadron result. At midrapidity, where $\langle x_2 \rangle$ is relatively large, the two parametrizations give rather similar results. As pointed out in Ref. [32], the difference between the kaon and proton ratios is due to isospin effects. As long as pion production is dominated by gluons, it is essentially independent of isospin. The ratio is greater than unity but smaller than the BRAHMS result at midrapidity. Including p_T broadening would increase the $|\eta| \leq 0.2$ ratio.

At $\eta=1$ and low p_T, the ratio is less than unity for both parametrizations but the stronger gluon shadowing in the FGS1 parametrization reduces $R_{d\mathrm{Au}}$ to ~ 0.8 for p_T
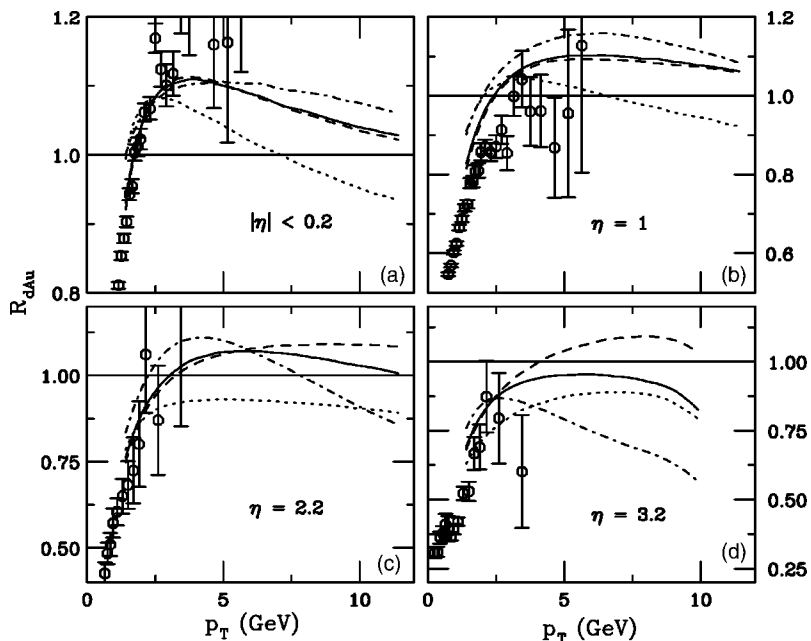

FIG. 2. $R_{d\mathrm{Au}}$ for charged pions (dashed) and kaons (dot-dashed) as well as protons and antiprotons (dotted) and the sum over all charged hadrons (solid) for deuteron-gold collisions at $\sqrt{S_{NN}}=200$ GeV as a function of p_T. The results for homogeneous shadowing with the FGS1 parametrization are compared to the minimum bias BRAHMS data [8] in the following η bins: (a) $|\eta| \leq 0.2$; (b) $\eta=1$; (c) $\eta=2.2$; and (d) $\eta=3.2$.
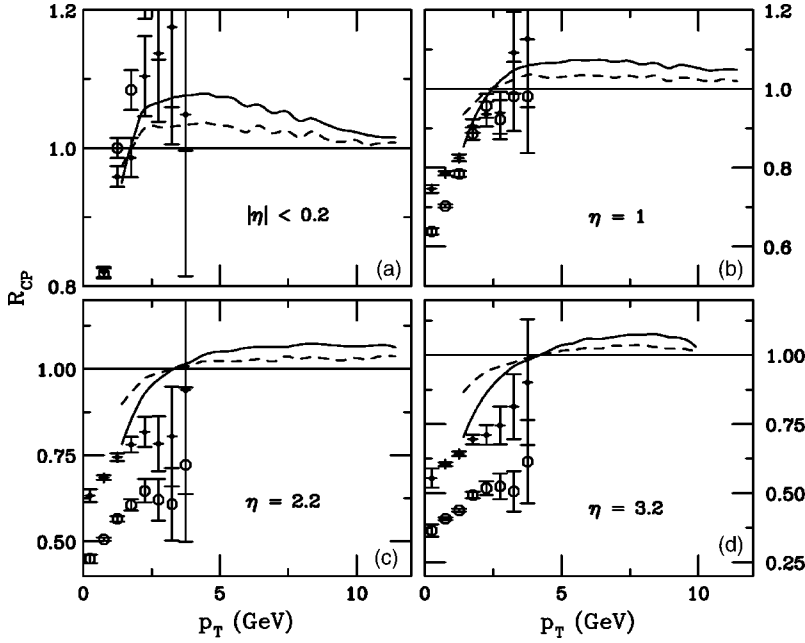
FIG. 3. R_{CP} for charged hadrons in deuteron-gold collisions at $\sqrt{s_{NN}}=200$ GeV as a function of p_T. The results for $S_{FGS1,\rho}$ are compared to the BRAHMS data [8] in the following η bins: (a) $|\eta|\leq 0.2$; (b) $\eta=1$; (c) $\eta=2.2$; and (d) $\eta=3.2$. The calculated ratios of the most central- and semicentral-to-peripheral collisions are shown in the solid and dashed curves, respectively. The BRAHMS data are given by the open circles (most central) and diamonds (semicentral).

$=\sqrt{2}$ GeV relative to ~ 0.9 for EKS98. At $p_T\sim 2.5$ GeV, R_{dAu} rises above unity again. At higher rapidities, R_{dAu} decreases at low p_T but does not rise as far above unity at higher p_T until, at $\eta=3.2$, the total charged hadron ratio is less than unity for all p_T. The EKS98 parametrization tends to underestimate the data for all but the most central rapidities; see Fig. 1. The FGS1 parametrization, on the other hand, agrees rather well with the central η data, Fig. 2(a), and lies within the errors of the most peripheral bins for $p_T>\sqrt{2}$ GeV, Figs. 2(c) and 2(d). However, the total charged hadron data at $\eta=1$ are somewhat underestimated by the FGS1 parametrization, Fig. 2(b).

In the most central bins, the ratio for the total charged hadrons closely follows R_{dAu} for the pions. At higher η, the kaon contribution becomes more important, causing the total to be closer to the average of the pion and kaon results. The proton contribution, on the other hand, remains small, even at $\eta=3.2$, while one may expect that, in reality, proton production would be more important at large rapidity as the fragmentation region is approached. However, this effect cannot be accounted for by standard parametrizations of the fragmentation functions. Since BRAHMS measures the negative charged hadron distribution h^- at $\eta=2.2$ and 3.2, only the antiprotons can contribute to R_{dAu}.

We point out that because x is not very small for p_T larger than a few GeV and the shadowing ratios are also not far from unity in this region, R_{dAu}, the ratios of $d+$Au relative to pp, are driven by isospin rather than shadowing. This is obvious from the very similar behavior of the EKS98 and FGS1 ratios seen in Figs. 1 and 2 for $p_T>5$ GeV.

Figure 3 illustrates the centrality dependence using $S_{FGS1,\rho}^j$. We compare the central-to-peripheral ratio R_{CP}, which should be less sensitive to isospin than R_{dAu}, to the BRAHMS data. The solid curves show the ratio of the central, (0–20)%, to peripheral, (60–80)%, bins for each η region while the dashed curves show the semicentral, (30–50)%, to peripheral ratios. Our calculations assume exact

impact parameter cuts while, experimentally, impact parameter is poorly measured on an event-by-event basis in d +Au collisions. We note that both of the inhomogeneous EKS98 results are much weaker than those in Fig. 3 and are not shown here.

In central collisions, with small impact parameter, inhomogeneous shadowing is stronger than the homogeneous result. The larger the homogeneous shadowing effect, the larger the difference between S_P^j and $S_{P,S}^j$. Thus R_{CP} is a stronger function of impact parameter for the FGS1 parametrization since it has larger homogeneous shadowing at small x. The ratios with $S_{EKS,S}^j$ underestimate the centrality dependence considerably and are not shown. Note that R_{CP} approaches unity at large p_T since the difference between S_P^j and $S_{P,S}^j$ decreases as x increases and the shadowing effect becomes small.

Since $S_{FGS1,\rho}^j(b)$ is a rather smooth function of impact parameter, the b dependence of R_{CP} is not very strong. The fluctuations in R_{CP} for $S_{FGS1,\rho}^j$, especially notable at central rapidity, are due to the discrete steps of $T_{Au}(r)$ in the integration over the spatial coordinates. These fluctuations are absent for $S_{P,WS}^j$ since $\rho_{Au}(r)$ is a smooth function.

The agreement with the data is reasonable at central η; see Figs. 3(a) and 3(b). The trends of the impact parameter dependence are similar to the data at low p_T. The semicentral-to-peripheral ratio is similar to the central-to-peripheral ratio in the most central rapidity bin while in the more peripheral bins, the central-to-peripheral ratio has a stronger p_T dependence. However, the increase in $\langle x_2\rangle$ with p_T results in the strong growth of R_{CP} with p_T at forward η. The resulting curvature of the calculated ratio is faster than the data. The magnitude of R_{CP} at low p_T is also underestimated. Since the position dependence of inhomogeneous shadowing is not well understood, the poorer agreement with the centrality-dependent data in Fig. 3 compared to the minimum bias results in Figs. 1 and 2 is not surprising. These

data could be used to tune the position dependence of shadowing.

In summary, we find that the suppression factor $R_{d\text{Au}}$, calculated with leading-twist shadowing, especially employing the FGS1 parametrization, agrees moderately well with the BRAHMS data. These calculations imply that saturation effects may not play a dominant role in the forward region at RHIC, as suggested in other recent work [33,34]. Our calculations of R_{CP} show a stronger p_T dependence than that suggested by BRAHMS, likely due to insufficient data on the impact parameter dependence of nuclear shadowing.

[1] PHENIX Collaboration, K. Adcox *et al.*, Phys. Lett. B **561**, 82 (2003); Phys. Rev. Lett. **88**, 022301 (2002).

[2] PHENIX Collaboration, S. S. Adler *et al.*, Phys. Rev. Lett. **91**, 072301 (2003); Phys. Rev. C **69**, 034910 (2004).

[3] STAR Collaboration, C. Adler *et al.*, Phys. Rev. Lett. **89**, 202301 (2002).

[4] STAR Collaboration, J. Adams *et al.*, Phys. Rev. Lett. **91**, 172302 (2003).

[5] BRAHMS Collaboration, I. Arsene *et al.*, Phys. Rev. Lett. **91**, 072305 (2003).

[6] PHENIX Collaboration, S. S. Adler *et al.*, Phys. Rev. Lett. **91**, 072303 (2003).

[7] STAR Collaboration, J. Adams *et al.*, Phys. Rev. Lett. **91**, 072304 (2003).

[8] BRAHMS Collaboration, I. Arsene *et al.*, nucl-ex/0403005, Phys. Rev. Lett. (to be published).

[9] M. Gyulassy, P. Lévai, and I. Vitev, Phys. Lett. B **538**, 282 (2002).

[10] I. Vitev, M. Gyulassy, and P. Lévai, Acta Phys. Hung. New Ser.: Heavy Ion Phys. **17**, 237 (2003).

[11] V. Emel'yanov, A. Khodinov, S. R. Klein, and R. Vogt, Phys. Rev. C **61**, 044904 (2000).

[12] R. D. Field, *Applications Of Perturbative QCD* (Addison-Wesley, Redwood City, CA, 1989).

[13] J. F. Owens, Rev. Mod. Phys. **59**, 465 (1987).

[14] S. R. Klein and R. Vogt, Phys. Rev. Lett. **91**, 142301 (2003).

[15] C. W. De Jager, H. De Vries, and C. De Vries, At. Data Nucl. Data Tables **14**, 479 (1974).

[16] D. Kharzeev, E. M. Levin, and M. Nardi, Nucl. Phys. **A730**, 448 (2004); L. Hulthen and M. Sagawara, in Handbüch der Physik, Vol. 39 (1957).

[17] A. D. Martin, R. G. Roberts, W. J. Stirling, and R. S. Thorne, Phys. Lett. B **443**, 301 (1998).

[18] M. Gluck, E. Reya, and A. Vogt, Z. Phys. C **53**, 127 (1992).

[19] K. J. Eskola, V. J. Kolhinen, and P. V. Ruuskanen, Nucl. Phys. **B535**, 351 (1998).

[20] K. J. Eskola, V. J. Kolhinen, and C. A. Salgado, Eur. Phys. J. C **9**, 61 (1999).

[21] L. Frankfurt, V. Guzey, and M. Strikman, hep-ph/0303022.

[22] CTEQ Collaboration, H. L. Lai *et al.*, Eur. Phys. J. C **12**, 375 (2000).

[23] T. Kitagaki *et al.*, Phys. Lett. B **214**, 281 (1988).

[24] V. Emel'yanov, A. Khodinov, S. R. Klein, and R. Vogt, Phys. Rev. C **56**, 2726 (1997).

[25] V. Emel'yanov, A. Khodinov, S. R. Klein, and R. Vogt, Phys. Rev. Lett. **81**, 1801 (1998).

[26] V. Emel'yanov, A. Khodinov, S. R. Klein, and R. Vogt, Phys. Rev. C **59**, R1860 (1999).

[27] A. L. Ayala, M. B. Gay Ducati, and E. M. Levin, Nucl. Phys. **B493**, 305 (1997).

[28] Z. Huang, H. Jung Lu, and I. Sarcevic, Nucl. Phys. **A637**, 79 (1998).

[29] B. A. Kniehl, G. Kramer, and B. Pötter, Nucl. Phys. **B582**, 514 (2000).

[30] STAR Collaboration, J. Adams *et al.*, nucl-ex/0309012.

[31] K. J. Eskola, H. Honkanen, V. J. Kolhinen, J. w. Qiu, and C. A. Salgado, Nucl. Phys. **B660**, 211 (2003).

[32] S. R. Klein and R. Vogt, Phys. Rev. C **67**, 047901 (2003).

[33] J. Jalilian-Marian, hep-ph/0402080.

[34] D. Kharzeev, Yu. V. Kovchegov, and K. Tuchin, hep-ph/0405045.